













A novel neurodevelopmental-neurodegenerative syndrome that cosegregates with a homozygous SPAG9/JIP4 stop-codon deletion

Natalia Acosta-Baena^{1,2} , Johanna Tejada-Moreno¹ , Alejandro Soto-Ospina^{1,2,3} , Alejandro Mejía-García¹ , Mauricio Preciado¹ , Jessica Nanclares-Torres^{1,2} , María Antonieta Caro¹ , Winston Rojas¹ , Gloria P. Cardona-Gómez² , Lucía Madrigal² , Mauricio Arcos-Burgos⁴ , and Carlos Andrés Villegas-Lanau^{1,2} 

This report outlines the clinical features of a complex neurological phenotype shared by three siblings from a consanguineous family, characterized by intellectual disabilities, speech developmental delay, gait disturbance, cerebellar syndrome signs, cataracts, and dysmorphic features (square and coarse facial features, thick lips, deep palate, small and spaced teeth, low-set ears, strabismus, eyelid ptosis, and blond hair). Seizures and brain atrophy were later evident. In the cosegregation analysis, five family members and 12 family controls were studied by whole-exome and Sanger sequencing. The structural and functional effects of the protein were explored to define the mutated variant's potential deleterious impairment. Neurological and neuropsychological follow-ups and brain magnetic resonance imaging (MRI) were performed. We identified a single frameshift homozygous nucleotide deletion in the SPAG9/JIP4 gene (NM_001130528.3): c.2742del (p. Tyr914Ter), causing a premature stop codon and truncating the protein and originating a possible loss of function. The variant cosegregated in affected individuals as an autosomal recessive trait. The *in silico* protein functional analyses indicate a potential loss of 66 phosphorylation and 29 posttranslational modification sites. Additionally, a mutated protein structure model shows a significant modification of the folding that very likely will compromise functional interactions. SPAG9/JIP4 is a dynein-dynactin motor adapter for retrograde axonal transport, regulating the constitutive movement of neurotrophic factor signaling and autophagy-lysosomal products. Under stress conditions, it can potentiate this transport by the p38 mitogen-activated protein kinases (p38MAPK) signaling cascade. Both functions could be associated with the disease mechanism, altering the axon's development and growth, neuronal specification, dendrite formation, synaptogenesis, neuronal pruning, recycling neurotransmitters and finally, neuronal homeostasis—promising common mechanisms to be used with investigational molecules for neurodevelopmental diseases and neurodegeneration.

Genomic Psychiatry (2024) 1, 1–12; doi: <https://doi.org/10.61373/gp024a.0052>; Published online: 5 August 2024.

Keywords: Intellectual disability, neurodevelopment, neurodegeneration, dementia, syndrome, axonal transport, retrograde signaling, signaling endosomes, MAPKp38 signaling pathway, dynein-dynactin motor adapter

Introduction

The molecular transport of molecules at the intracellular level is essential to a cell's development and survival (1). This challenge for neurons is permanent due to the everlasting and distant polarization between the axons and the neuronal body. However, distance is not the only challenge; localized delivery of presynaptic components must be successfully overcome to maintain synaptic transmission (2). To carry out this process, neurons use "axonal transport" to ship multiple substances that move along the microtubules of the axon in a bidirectional way (3, 4).

The kinesin complex drives anterograde movement transport (from the soma to the axon tip) and ships transport substances such as RNA, proteins, and organelles to growth cones and synapses (5). The opposite, retrograde movement (from the axon to the neuronal body), is dynein dependent and important for neurotrophic factor signaling (6), autophagy-lysosomal-autophagy, degradation, and nerve regeneration. The machinery for this axonal transport includes motor and microtubule proteins and essential adapters (7). Furthermore, protein kinase signaling pathways and posttranslational microtubule modifications are required to ensure efficient transport into neurons (2).

Alterations in axonal transport can emerge through several mechanisms: (1) defects in the organization of the cytoskeleton, (2) alterations in the binding of motor proteins to microtubules, (3) abnormal kinase or dynein activities, (4) destabilization of motor cargo binding, and (5)

alterations in mitochondrial dysfunction energy (8). Thus far, inadequate and nonprogressive retrograde movements can disrupt synapses, axonal growth, plasticity, and neuronal homeostasis. Multiple neurological diseases are associated with axonal transport disorders (7, 9).

The JIP4 protein, encoded by the SPAG9 gene, is a dynein-dynactin motor adapter that favors axonal retrograde flow. JIP4 is ubiquitously expressed, including the central and the peripheral nervous system (10). Protein expression studies in brain-derived neurodevelopment axons have shown high levels of JIP4, which are detected in lysosomal fractions and autophagic vacuoles (11). JIP4 promotes and stabilizes the association with dynactin while antagonizing kinesin binding (12). Thus, in a mutually exclusive manner, retrograde transport is activated. JIP4 is involved in postnatal brain development (13) and neuronal homeostasis by intracellular metabolites recycling to maintain neuronal homeostasis (14). In humans, SPAG9/JIP4 has been associated with the prognosis of different types of cancer (15) but never linked to intellectual disability and/or complex neurodevelopmental phenotypes.

This article describes three homozygous siblings with a mutant variant of the SPAG9 gene, affected by a complex phenotype characterized by developmental and language delay, severe learning difficulties, and motor compromise impairment. The follow-up of this family for more than 10 years has also suggested a cognitive deterioration progressive impairment, suggesting a subsequent neurodegenerative process. Preliminary findings were presented on a poster (16).

¹Grupo de Genética Molecular (GENMOL), Universidad de Antioquia, Medellín, Colombia; ²Grupo de Neurociencias de Antioquia (GNA), Facultad de Medicina, Universidad de Antioquia, Medellín, Colombia; ³Grupo de Investigación en Alimentos (GRIAL), Facultad de Ingeniería, Corporación Universitaria Lasallista, Caldas, Colombia; ⁴Grupo de Investigación en Psiquiatría (GIPSI), Departamento de Psiquiatría, Instituto de Investigaciones Médicas, Facultad de medicina, Universidad de Antioquia, Medellín, Colombia.

Corresponding Author: Natalia Acosta-Baena, Universidad de Antioquia, Facultad de Medicina, Grupo de Neurociencias de Antioquia (GNA), SIU, Sede de Investigación Universitaria, AA1226, Calle 62 Número 52-59, Medellín, Colombia. Phone/Fax: 57-4-2196444. E-mail: natalia.acosta@gna.org.co

Received: 6 March 2024. Revised: 6 June 2024. Accepted: 19 June 2024.





Methods

Study Site and Family

This study was carried out at the “Universidad de Antioquia,” Medellín, Colombia, in collaboration between The Grupo de Neurociencias de Antioquia (GNA) and Genética Molecular (GENMOL) research groups. The bioethics committee of the university (Comité de Bioética, Sede Investigación Universitaria CBE-SIU) approved the protocol study. The subjects who were studied signed the informed consent form after a detailed explanation of the objectives and procedures of the study. In cases where the subject did not know how to sign, parents or representatives gave consent and signed the form. The family was identified in Antioquia, Colombia, in 2011 and clinically followed up with subsequent follow-ups until 2021.

Characterization of the Phenotype

The physician’s team from the GNA carried out medical, neurological, and psychiatric follow-ups. Laboratory tests, brain magnetic resonance imaging (MRI), and neuropsychological evaluations were performed on the cases. Affected individuals were evaluated at a medical school pediatric-neurology meeting staff at the university hospital to discuss the complex phenotype and to consider some potential differential diagnoses. The neuropsychological evaluations were carried out using the GNA protocol, and the Wechsler Intelligence Scale (17) was additionally included. The severity of the cases was assessed using a comprehensive battery of structured and semi-structured clinical tools based on the DSM-5 criteria, according to IQ measures and functional performance scale assessment in daily life. Acquired dementia or cognitive impairment was diagnosed according to established standard criteria using neurological and neuropsychological evaluation tools and family reports. A more detailed description of these instruments is presented elsewhere (18).

Genetic Analysis

DNA extraction followed a standard extraction protocol with the peripheral blood samples using the salting out method (19), and the samples were stored at -20°C until sequencing. MacroGen performed the whole-exome sequencing (WES). The coding regions of the genome were sequenced by next-generation sequencing using the Illumina platform with an average coverage of 100X. The SureSelectXT Library Prep Kit (Target Enrichment System for Illumina Version B.2, April 2015) enriched the library (20). Sequencing was performed on a HiSeq 4000 instrument following the standard protocol to reach a 100X deep read average. The data were processed using the HCS software [HiSeq Control Software (HCS 3.3) version 3.3]. Sequencing data were converted to the FASTQ format using the Illumina package bcl2fastq module [version 2.16.0.10 from Illumina (21)]. The bioinformatic analysis was carried out with these data afterward.

Bioinformatic Analysis

The quality of the reads was evaluated with the fastqc v0.11.5 tool from the Babraham Institute, <http://www.bioinformatics.babraham.ac.uk/projects/fastqc> (22). Subsequently, the sequences were mapped to the hg19 reference genome available at the University of California, Santa Cruz (UCSC) website, <http://hgdownload.cse.ucsc.edu/goldenpath/hg19/chromosomes/> using the Burrows-Wheeler Aligner, as implemented in the bwa-0.7.12 software, <http://bio-bwa.sourceforge.net/> (23). Variant calling was performed using the Broad Institute’s Genome Analysis Tool Kit GATK tool (GATK) v3.8-1 Best Practices for Germline SNP & Indel Discovery in the Whole Genome and Exome Sequence <https://software.broadinstitute.org/gatk/> (24). For the process of marking duplicates, the Picard v1.119 tool <https://broadinstitute.github.io/picard/> was used. Base recalibration processes (BQSR – base quality score recalibration), the search for single-nucleotide polymorphism (SNP)-type variants and INDELS (variant calling) and variant filtering (hard filtering) were carried out considering the protocol suggested by the tool GATK (Genome Analysis Tool Kit) from the Broad Institute (Best Practices for Germline SNP & Indel Discovery in Whole Genome and Exome Sequence) <https://software.broadinstitute.org/gatk/best-practices/bp3step.php?case=GermShortWGS>. Once the variants were identified, the annotation was carried out with the wANNOVAR (25) and Ensembl Variant Effect Predictor programs (26), which make use of the

information collected in different databases and bioinformatic tools for the search of the allelic frequencies of the variants in the different continental populations such as 1000 Genomes, ExAC, ESP6500 and gnomAD.

The clinical interpretation of genetic variants was considered by the guidelines proposed by the American College of Medical Genetics and Genomics and the Molecular Pathology Association (ACMG) (27). The tools InterVar (28) <http://wintervar.wglab.org/> and VarSome (29) <https://varsome.com/> were used to classify each of the identified candidate variants.

The variants were prioritized considering the following criteria: (1) Quality of the sequences: Depth across samples ($DP > 30$). (2) Mode of inheritance: autosomal recessive. (3) Allelic frequency (MAF < 0.01) in a population database (1000 Genomes, ExAC, ESP6500, gnomAD). We filtered only variants with a frequency less than 0.01 with a higher probability of causing major effects and rare Mendelian conditions. (4) Exonic variants or variants at splicing sites were included. (5) Pathogenic variants, probably pathogenic or variants of uncertain significance—VUS—were also included. (6) Pathogenicity predictors: variants cataloged as deleterious or possibly deleterious by more than three pathogenicity predictors, including, that is, SIFT, and PolyPhen2 Polyphen2, and presenting with values higher than 14 by the CADD predictor, and (7) The potential relationship with the phenotype by considering Human Phenotype Ontology terms were evaluated.

Sanger Sequencing

The variant identified was replicated using Sanger sequencing in four samples: two affected individuals with DNA available and both parents. FinchTV version 1.4.0 (Geospiza, Inc.; Seattle, WA, USA), <http://www.geospiza.com/Products/finchtv.shtml> was used to evaluate the quality of the chromatograms. We used Aliview version 1.18 <http://www.ormbunkar.se/aliview/> (30) and novoSNP version 3.0.1 <http://www.molgen.ua.ac.be/bioinfo/novosnp> (31) to identify and analyze candidate variant.

Functional and Structural Analysis

The bioinformatics study began with the analysis of the primary sequence in FASTA format to characterize the system from the potential perspective of posttranslational protein modifications considering the calculation of N-glycosylation of amino acids with amide groups in their side chain, from the probability as estimated by measured with the NetGlyc 1.0 server software.

Similarly, the interaction of O-glycosylation sites by the OH functional group was measured with the NetOglyc 4.0 server software. Likewise, the phosphorylation patterns were measured with the NetPhosK 3.1 server software for the amino acids whose side chain is serine, threonine, or tyrosine is present in the sequence of the evaluation of 17 kinases: ataxia-telangiectasia (ATM), creatine kinase I (CKI), creatine kinase II (CKII), Ca^{2+} /calmodulin-dependent protein kinase II (CaM-II), DNA-dependent protein kinase (DNA-PK), epidermal growth factor receptor (EGFR), epidermal growth factor receptor-3 (GSK3), insulin receptor (INSR), protein kinase A (PKA), protein kinase B (PKB), protein kinase C (PKC), protein kinase G (PKG), ribosomal S6 kinase (RSK), Src family kinases (SRC), cell division cycle gene in *Schizosaccharomyces pombe*, named *cdc1* in mammals (*cdc2*), cyclin-dependent kinase 5 (*cdk5*), and p38 mitogen-activated protein kinases (p38MAPK) (32–34).

To identify the three-dimensional structure of SPAG9, portions of the protein sequence were searched for in the Protein Data Bank. The analyzed structure by X-ray diffraction with a resolution of 1.80 Å was constituted by 70 amino acids (ID: 2 W83). This structural fragment was used as a template for the complete model (35).

To model the protein structures of the SPAG9 and the SPAG9 Tyr914Ter variants, three-dimensional SPAG9/JIP4 wild-type, as well as other likely structures, were obtained from the AlphaFold repository built by the DeepMind-Evoformer module (36). Five models with a significant spatial arrangement convergence as measured by the local distance difference test (37) were chosen. The machine learning modeling allowed the reconstruction of the truncated protein encoded by the SPAG9 Tyr914Ter variant. From the five models, we selected the one with the best molecular score (38). The global alignment between the wild-type and the

**Table 1.** Clinical characteristics of affected individuals

	Case 1	Case 2	Case 3
Age at exam, years	36	34	32
Gender	M	F	F
Height (cm)	165	168	172
Body Mass Index	27.5	29.1	24
Head circumference (cm)	57	58	58
Facies and general characteristics	Blond hair, thick lips, coarse facial features, square face, deep palate, low-set ears, spaced teeth. Single palmar crease, pes cavus.		
Skin	Hyperpigmented macules in the periorbital region and face	Hyperpigmentation in periorbital region	—
Reported dyslipidemia	+	+	—
Other pathologies	—	—	Asthma, rhinitis
Delayed psychomotor development/ Intellectual disability	+	+	+
Language disturbance	+	+	+
Cataracts	+	+	+
Strabismus	+	+	+
Eyelid ptosis	Bilateral	Unilateral (left)	—
Seizures	Seizures from 34 years of age	—	—
Gait disturbance	Scoliosis. Walk with both feet apart and with the balls of the feet with external deviation	Impaired tandem gait, slight outward deviation of the balls of the feet	Impaired tandem gait
Parkinsonism	—	—	—
Cerebellar syndrome (intention tremor, dysdiadochokinesia, ataxia, dysmetria)	Ataxia	Dysmetria	Dysmetria and dysdiadochokinesia
Dystonia	+	—	—
Dysarthria	—	—	—
Impaired coordination	+	+	+
Pathological reflexes	Sucking reflex	—	Sucking reflex
Plantar reflexes	—	—	—
Urinary incontinence	+	—	—
Supranuclear palsy	—	—	—
Nystagmus	+	+	—
Psychiatric symptoms/behavior	He pulls out his nails and teeth. Aggressiveness.	Apathy, abulia, compulsion to eat	Irritability and disinhibition
Superior member			
Spasticity	—	—	—
Weakness	—	—	—
Hyperreflexia	—	—	—
Sensory disability	—	—	—
Lower member			
Spasticity	—	—	—
Weakness	—	—	—
Hyperreflexia	—	—	—
Sensory disability	—	—	—

mutant protein models was achieved with the Needleman Wunsch algorithm applied to the BLOSUM62 matrix and quantifying the RMSD standard deviation between the models. The three-dimensional models were pictured with the Chimera U.C.S.F visualizer v 1.1.1 (39).

Results

Clinical Description of the Affected Siblings

Two parents and three affected children constitute the nuclear family. Table 1 details the summary of clinical findings for each individual.

Case 1. Male, firstborn, 40 weeks, normal pregnancy. Spontaneous vertex delivery without any complications. Average weight at birth. At 1 year of life, significant motor delay development of bilateral eye cataracts. Head support is at 4 years old, but walking is difficult. He could not chew and swallow food until he was 6 years old, for which he was fed only with blended food. The first two words, “mama” and “papa,” are at 4 years old. At the age of 30, the development of complete oral sentences begins. At

34 years old, development of generalized tonic-clonic seizures. Entirely dependent on all daily living activities but with behavior changes in recent years. He pulled out his nails and his teeth aggressively. Functional scales have deteriorated over time.

Case 2. Female, second pregnancy product, without significant prenatal or perinatal history. Spontaneous vertex delivery without any complications. Hold the head and trunk up at 8 months old. Walking and pronunciation of first words around 16 months old. Severe learning and mental disability (only can sign). Currently, she pronounces only three words. She is independent in daily life functions and helps her mother with simple household tasks.

Case 3. The third average pregnancy female product. Spontaneous vertex delivery without any complications. Sitting at 10 months old, walking age at 15 months old, and first words at 24 months old. Developed bilateral cataracts at 4 years old. Mild motor and learning delay development.

**Table 2.** Summary of neuropsychological assessment of affected individuals

Cognitive function	Case 1	Case 2	Case 3
Mini-Mental State Examination (MMSE)/30	6	13	19
Orientation	Far below average	Far below average	Below average
Verbal fluency/denomination	0	7	In the average age and schooling
Word list memory/10	0	1	5
Evocation memory/10	0	1	3
Visual memory	Cannot take the test	Cannot take the test	Far below average
Attention	Cannot take the test	Cannot take the test	Cannot take the test
Executive function	Cannot take the test	Cannot take the test	Cannot take the test
Visuoconstructive function	Cannot take the test	Cannot take the test	Cannot take the test
Apraxia	+	+	+
Full scale IQ	45	45	45
Verbal IQ	48	50	49
Performance IQ	47	47	47

She works as a laundress in a dairy—recent years with marked disinhibition.

Neuropsychological Assessment. The three siblings were classified with moderate intellectual disability according to the DSM-5 criteria, and all three obtained an IQ score of 45 (Table 2).

Brain Imaging. Brain MRI was performed for all affected individuals. The MRI results show heterogeneity between all of them (Figure 1). There was no cortical dysplasia or polymicrogyria in any of the cases. Tractography by diffusion tensor imaging are normal. Cochlea, vestibule, and brainstem are normal. In all three siblings, there is mild microangiopathy (Fazekas scale grade 1 for deep white matter). Ventriculomegaly is predominantly left, with slight prominence of the sulci of the upper cerebellar vermis. It draws attention to decreased iron deposits in the globus pallidus and a slight increase in the putamen, being more significant in case 3. Case 1 attracts attention for microcephaly, decreased fronto-occipital diameter according to biometric parameters by age and sex (Figure 1A) (40). The hypoplastic corpus callosum (CC) without dysplasia, with a decreased thickness of the genu (40). Bilateral hippocampal malrotation with both collateral sulci are vertical (Figure 1B). Slight iron deposit in the putamen. Case 2 with lower limit frontal-occipital diameter and decreased thickness of the genu of CC, left hippocampal malrotation. In case 3, we additionally see malrotation of the left hippocampus. The putamen nucleus is seen with more significant iron deposits, and unlike the other cases, there is agenesis of the septum pellucidum (Figure 1B). Also, there is a very thin CC, mainly the splenium. Loss of subcortical volume, with a more dilated fourth ventricle and increased iron deposits in the dentate nucleus.

Identification, Clinical Interpretation, and Validation of Candidate Variants

The complete family included 36 members. Three affected siblings and their two parents were available for WES. We extend the analyses to the remaining family members, available in 17 individual exomes. A homozygous deletion in the SPAG9 gene (*NM_001130528.3*): *c.2742del (p. Tyr914Ter)* was identified in the three affected siblings-heterozygous in their parents and a maternal uncle. This variant has not been found in other family members and disparate populations according to 1000 Genomes, ExAC and GnomAD databases. It has not been found in exomes (coverage: 86.8) and genomes (coverage: 31.7), according to VarSome (29). Figure 2 shows the complete genealogy and the results of the Sanger sequencing of the four individuals.

Structural and Functional Analysis of the SPAG9/JIP4 Model Protein and Its Relationship with the SPAG9Tyr914

The SPAG9/JIP4 protein is expressed at the cytoplasmic level and in the cell lysosome, belongs to chromosome 17 and has a mass of 146,205 (Da). It has six isoforms, and the isoform with the highest frequency related to the interaction with kinesin is the isoform with a composition of 1321

amino acids (41–43). It binds to dynein and kinesin-1 in the leucine zipper II (JIP LZII) domain (Figure 3), allowing bidirectional vesicular transport along the microtubules and their dynamics (44).

The mutation found at position 914 is associated with a nucleotide change that produces a termination codon due to guanine (G) deletion. This stop codon prevents the protein from extending further and causing loss of structural information, but it directly affects the three-dimensional arrangement. Therefore, the protein presented changes in length and amino acid composition due to the lack of assembly of 407 amino acids. In the characterization of the system, the effect on the post-translational modifications that the protein can undergo and the changes it can generate were analyzed. Calculation of phosphorylation sites, O-glycosylation and N-glycosylation sites were made from the primary sequences to characterize the two proteins, as shown in Table 3.

For SPAG9wt, there are 257 phosphorylation sites in total (Table 4). The repeated numbers are due to their being phosphorylated by various kinases at the same position when they exceed the normalized phosphorylation value of 0.500. The mutation identified at position 914, which, in this case, produces a stop codon, means that the protein cannot extend further and loses structural information, which directly affects the three-dimensional arrangement. Regarding phosphorylation, due to the spatial effect from position 909, the phosphorylations considered up to the total SPAG9 protein with 1321 amino acids were lost (Table 4). These kinases contemplate positions with a triple possibility of phosphorylation, such as position 1188 with a nonspecific enzyme and two essential enzymes (protein kinase A and protein kinase C) involved in cell signaling. In the same way, position 1238 with the kinases p38MAPK, cdk5 and GSK3; position 1249 with a nonspecific enzyme, protein kinase C and cdc2; similarly, position 1262 with a nonspecific enzyme, DNA-PK and ATM. Finally, position 1264 has phosphorylation loss of a nonspecific enzyme, cdk5 and p38MAPK.

Regarding the O-glycosylations, 106 glycosylation sites were considered for SPAG9wt, which considered a probability greater than the threshold at 0.5. When the SPAG9 Tyr914Ter mutation occurred, there was a decrease in the total number of O-glycosylation sites, among which changes appeared in the N-terminal amino acid residue due to the effect of the change in spatial arrangement with position 16. These changes conceive effects by early protein termination and loss of glycosylation for positions 905, 909, 911, 915, 937, 938, 949, 1179, 1188, 1238, 1241, 1242, 1243, 1244, 1246, 1249, 1256, and 1262. These alterations in O-glycosylation affect protein polarity and the adhesion of other circulating protein systems. N-glycosylation was also a highly affected post-translational modification. Six modifications were made at positions 309, 565, 694, 830, 939, and 1176, but due to the mutation SPAG9 Tyr914Ter, only one modification was performed at position 309. Molecular modeling allowed us to obtain the SPAG9wt protein, as shown in Figure 4A and the variant with the stop codon in three-dimensional alignment with the native structure, in Figure 4B.

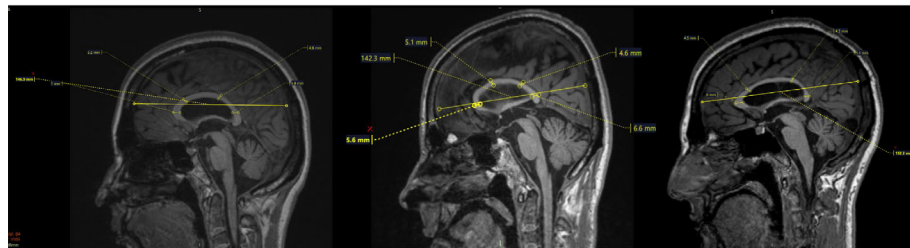


(A) 1.

Case 2

Case 1

Case 3



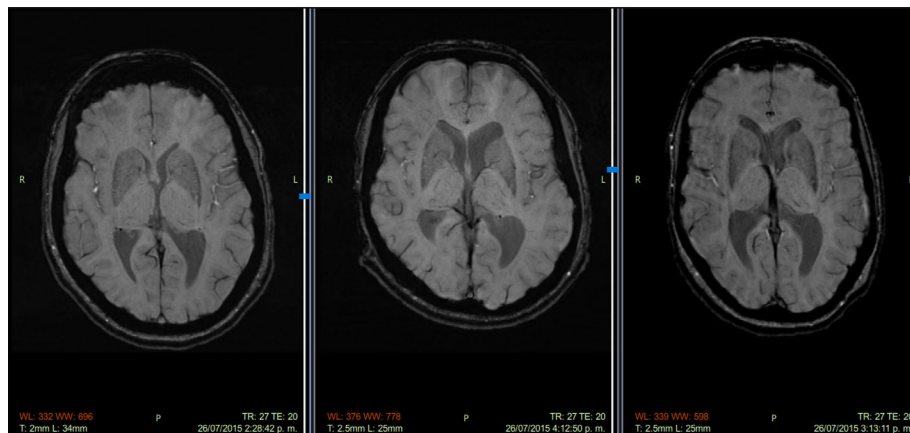
	FOD	3rd Perc	GT	3rd Perc	BT	3rd Perc	IT	3rd Perc	ST	3rd Perc
Case 1	142.3	154	5.6		5.1		4.6		6.6	
Case 2	146.9		7.0	7.6	5.2	3.7	4.6		5.8	6.3
Case 3	152.2	148.3	8.0		4.5		4.2		5.1	

(A) 2.

Case 2

Case 1

Case 3



(A) 3.

Case 2

Case 1

Case 3

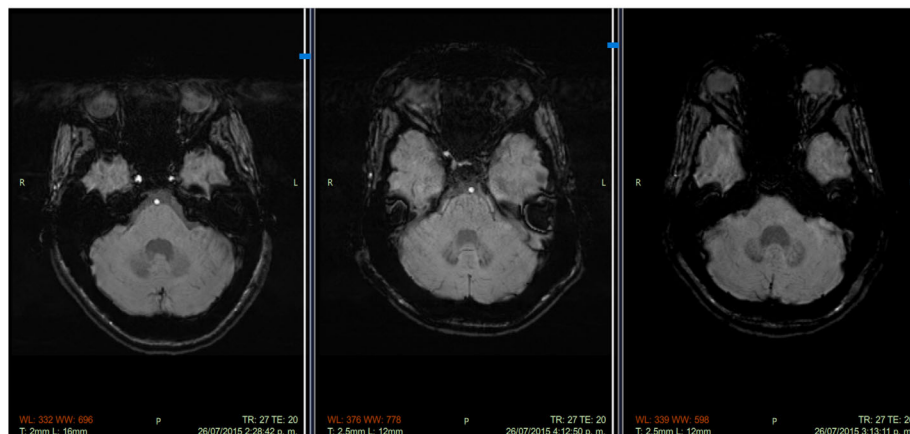
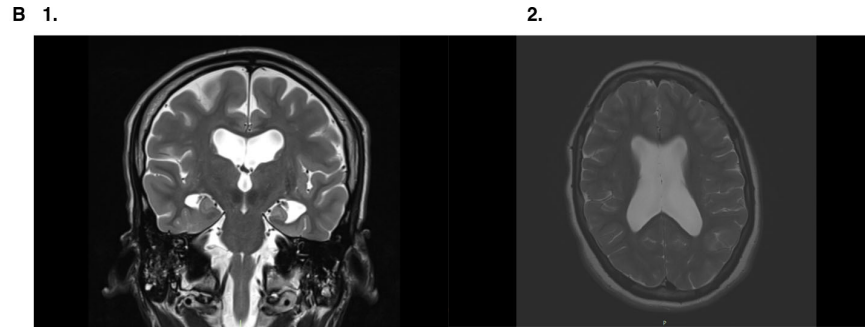


Figure 1. Findings reported on brain MRI of three siblings. (A) Comparison between the three cases according to 1. Measurements of the fronto-occipital diameter (FOD) and parameters of the CC (GT: Thickness of the genu, BT: Thickness of the body, IT: Thickness of the isthmus, ST: Thickness of the splenium) 2. Gradient of iron deposits in the putamen nucleus, from lowest to highest, with case 3 being highest. 3. Cerebellum and fourth ventricle. (B) 1. Bilateral malrotation hippocampal (Case 1). 2. Agenesia of the septum pellucidum (Case 3).

Discussion

This study reports a new syndrome with congenital alterations, neurodevelopment disorder, and neurodegeneration. The exomes analyzed from 17 family members, Sanger segregation analysis, and structural and functional evidence help determine possible pathogenic variants with significant effects. With the observations presented, we can conclude that

this rare disease can be associated with the homozygous deletion of SPAG9/JIP4 gene. The family was identified from the rural area of northern Antioquia, Colombia, where a genetic isolate was previously reported, with a founder effect and several genetic disorders associated with a possible genetic bottleneck (45–47).



	Microcephaly	Hippocampal malrotation	Corpus callosum Hypoplastic	iron deposit (Putamen - dentate nucleus)	Cerebellar atrophy (Upper vermis)	Agenesis of the septum pellucidum
Case 1	+	Bilateral	+	+	-	-
Case 2	+	Unilateral	+	+	-	-
Case 3	-	Unilateral	++	++	+	+

Figure 1. (Continued)

These three siblings present similar clinical characteristics. They had close scores on the intelligence scale (IQ) despite such a dissimilar Mini-Mental State Examination (MMSE), probably because of the differences in language. In other aspects, we can see heterogeneity in severity despite having the same mutation. The male case is the one who has the

most severe motor disorder, with more incredible difficulty in language and functionality, in addition to severe psychiatric symptoms and facial dysmorphism. The younger sister (case 3) appears to have other essential alterations on MRI. However, functionally, she performed better in daily living activities and revealed minor differences in facial features.

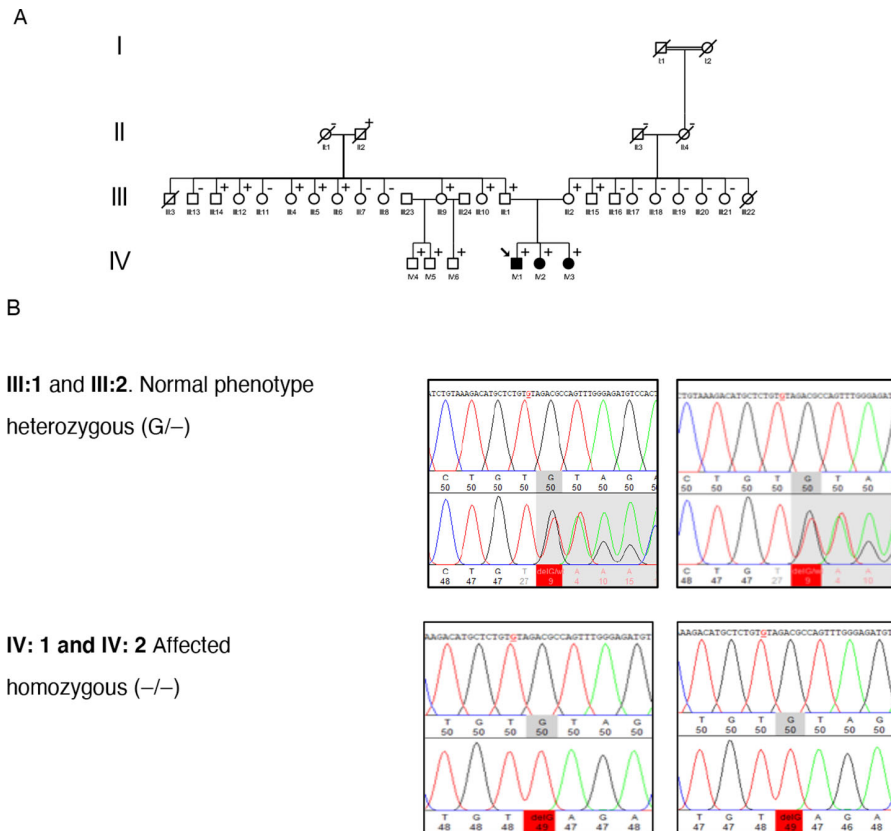


Figure 2. Family's pedigree and Sanger sequencing. **(A)** Pedigree shows four generations of the complete family. Squares are men, and circles are women. The arrow indicates the index case. Roman numerals are generations, and Arabic numerals represent the position of each individual in the family. Filled squares and circles represent affected family members. Slash (/) indicates a deceased person. The same line between two individuals represents consanguinity. Individuals with DNA samples are indicated with a plus (+) symbol. **(B)** Chromatograms of three subjects (parents and two siblings) were available and visualized with novoSNP (31). The reference sequence is visualized in the first trace. Variation is highlighted in red color. The unaffected parents III: 1 and III: 2 are heterozygous (G/-), and the two affected children IV: 1 and IV: 2 are homozygous (-/-) for the variant (*NM_001130528.3*): c.2742del.

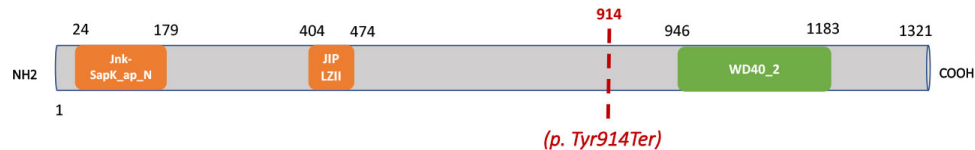


Figure 3. Localization of (*NM_001130528.3*): *c.2742del (p. Tyr914Ter)* in the domains of the SPAG9/JIP4 protein. Scheme of the SPAG9/JIP4 protein with the main domains and the location of the identified variant.

According to the MRI, microcephaly and bilateral hippocampal malrotation in case 1 were evident. Hippocampal rotation can begin between gestation weeks 21–32. Asymmetrical development is expected, with the right side faster than the left (48). A malrotation or incomplete inversion of the hippocampus can be expected in 19%. However, it can also be associated with structural variants associated with brain development that predispose to epilepsy to some extent (49). It is striking that this case has been the only one of the three siblings who has presented convulsive episodes after the age of 34.

The CC is the main structure that connects the cerebral hemispheres and integrates motor, cognitive, and sensory information. Morphological anomalies correlate with alterations in cognitive and behavioral development. Each subregion (genus, body, isthmus, and splenium) is associated with development and function in the cortex. We observed a decrease in the size of the genu and splenium. Genu are projections from the prefrontal cortex. The splenium has fibers from the occipital-parietal and temporal cortex (50). Full maturity of the CC appears to occur in early adulthood. It has been suggested that the increase in CC size at that age is related to the increase in axonal size (51). In all three cases, there is ventriculomegaly, possibly associated with subcortical atrophy and iron accumulation in the putamen and the dentate nucleus. Findings that could be associated with neurodegenerative changes. Iron is the most abundant metal in neurons; transport and storage failures are processes associated with neurodegenerative disorders (52). It is interesting to explore these findings further since they would provide clues to mechanisms not yet understood in dementia syndromes.

These cases were identified in the fourth decade of life, so we can observe the evolution of a neurodevelopmental disorder whose cause remains and appears to be progressing. In subsequent evaluations, all siblings had worsened in the functional scales (data not shown) and brain atrophy. Also noteworthy is the onset of seizures at age 34 and worsening motor and behavior impairment in case 1. Aspects that suggest possible degeneration after the developmental disorder.

Our findings conclude that deletion in the SPAG9 gene (*NM_001130528.3*): *c.2742del (p. Tyr914Ter)* generates changes in the protein regarding length and amino acid composition due to lack of assembly of 407 amino acids. This affects posttranslational modifications, affecting key sites for N-glycosylation, O-glycosylation, and phosphorylation. These three-dimensional effects and modifications are responsible for changing the chemical environment of the protein, which implies an alteration in cell function, either by activating a metabolic pathway or cell signaling, such as the interaction with cofactors and ligands such as dynein and kinesin-1, among others. The identified homozygous deletion produces a double truncated protein, with the absence of important kinase phosphorylation sites, including two positions for p38MAPK, in addition to the absence of 24 sites for O-glycosylation and five sites for N-glycosylation for its proper function.

JIP4 protein has two known molecular functions: (1) Dynein-dynactin motor adapter for retrograde flow. (2) Scaffold protein that potentiates the p38MAPK signaling cascade. Murine studies with a double knockout (KO) to JIP4 have shown neurodegeneration (11), but no previous cases with this phenotype associated with JIP4 mutations had been reported. The alterations in neurodevelopment and neurodegeneration seen in our patients could be explained by permanent alteration retrograde axonal transport and signaling deficiencies p38MAPK cascade.

p38MAPK regulates several cellular functions in the central nervous system, such as metabolism, secretion, migration, differentiation, apoptosis, and senescence (53). The cascade consists of three phosphorylation

levels to activate p38, starting with a MAP kinase (MAP3K), then a MAP2K, and finally p38 MAP kinase. Protein kinases regulate axonal transport by phosphorylating motor and adapter proteins and cargoes directly and indirectly by modifying the microtubule network (54). MAPKp38 can negatively regulate axonal transport. In patients and mice with amyotrophic lateral sclerosis (ALS), overactivation of this signaling pathway produces alterations in axonal transport in the spinal cord (55). Scaffolding proteins, such as JIP4, recruit upstream MAP2K and MAP3K to enhance the activation of p38 kinases (10). JIP4 regulates retrograde and constitutive transport of lysosomes, but under stress conditions, it activates the p38 MAPK signaling pathway with posttranscriptional regulation of TMEM55B. TMEM55B recruits JIP4 to deliver dynein-dynactin to lysosomal membranes (56). Depletion of TMEM55B or JIP4 results in the dispersal of lysosomes toward the cell periphery (57). More research is required to understand alterations in JIP4 and their impact on regulating mTORC signaling (58).

The shortening of the protein was before the position of the WD40 domain (12). Proteins with this type of domain are associated with the function of interacting with other proteins (59). This domain would give its scaffolding function, which is fundamental to critical functions in signaling pathways and the gathering of multiple partners to facilitate concerted interactions and molecular functions. Functional studies are required to determine the implications of these findings for regulation, cell types or specific tissues, and machinery involved in each process where retrograde transport is involved.

The JIP4 homologous protein, previously identified as JIP3, overlaps with JIP4 in regulating axonal lysosome transport in neurons (60). According to previous studies, it has been suggested that JIP3 and JIP4 are functionally redundant and whose main difference is the expression of JIP3 only in neuronal cells (14). It has been hypothesized that if JIP3 is not expressed, JIP4 can replace JIP3 in the kinesin activation complex (14). De novo heterozygous mutations in the MAPK8IP3 gene encoding the JIP3 also show a phenotype of intellectual disability and brain abnormalities (61, 62). The reported variants are located in the four main domains of the JIP3 protein, including three mutations within the WD40 domain (62). Here, we report these first three cases with possible pathogenic mutations in JIP4, which demonstrate the importance of JIP4 at the brain level despite the presence of JIP3. This could agree with the statement that JIP4 has different functions than JIP3, and its presence is essential and not replaceable in certain brain functions or signaling pathways (10).

Retrograde endosomal signaling in neurons includes the following steps: internalization of ligand–receptor complexes into axon terminals, sorting of complexes into active signaling vesicles, transport along axonal microtubules to cell bodies, signaling endosomal and the dismantling of the complex (63). The central motor for retrograde transport is a cytoplasmic dynein complex composed of multiple subunits. This complex binds to microtubules and hydrolyzes ATP. However, on its own, it cannot carry out transport without dissociating from microtubules, so it depends on adapter proteins for efficient processivity (9).

How Does Defective Retrograde Axonal Transport Contribute to Neurodevelopmental Disorders?

Retrograde intracellular communication is essential for brain development and maintenance (2). The neurotrophin family of growth factors are synthesized and secreted away from neuronal cell bodies, propagate retrogradely along the axon to the body of the neuron and are required for proper neuronal survival, axonal growth, gene expression, neuronal



Table 3. Phosphorylation and posttranslational modifications sites in wild-type SPAG9 and SPAG9 Tyr914Ter

Protein	Phosphorylation sites	O-glycosylation sites	N-glycosylation sites
wild-type SPAG9	257 phosphorylation sites: Positions 9, 21, 21, 25, 30, 30, 32, 87, 109, 109, 109, 119, 119, 119, 123, 123, 126, 126, 143, 143, 183, 183, 183, 185, 185, 194, 194, 203, 203, 217, 217, 226, 226, 238, 238, 242, 244, 245, 245, 249, 251, 268, 268, 268, 268, 268, 272, 272, 275, 276, 276, 276, 279, 283, 292, 305, 305, 329, 330, 332, 332, 332, 339, 339, 339, 347, 347, 347, 348, 358, 363, 363, 364, 365, 379, 381, 381, 381, 387, 388, 391, 391, 418, 493, 493, 497, 504, 504, 504, 538, 538, 550, 550, 550, 551, 551, 551, 557, 561, 561, 562, 563, 564, 564, 564, 566, 566, 567, 567, 578, 582, 582, 583, 586, 586, 588, 588, 593, 593, 594, 594, 594, 595, 595, 595, 597, 611, 614, 617, 620, 620, 629, 683, 684, 705, 705, 710, 713, 728, 730, 730, 730, 732, 732, 733, 733, 756, 763, 764, 790, 804, 804, 806, 806, 813, 815, 822, 826, 829, 831, 832, 835, 837, 837, 848, 858, 858, 858, 858, 858, 861, 865, 865, 865, 879, 879, 887, 892, 895, 901, 901, 905, 909, 909, 909, 932, 935, 937, 944, 944, 966, 966, 967, 986, 996, 996, 1002, 1021, 1036, 1049, 1049, 1054, 1054, 1069, 1081, 1081, 1090, 1090, 1105, 1110, 1111, 1111, 1131, 1138, 1144, 1149, 1149, 1169, 1173, 1175, 1188, 1188, 1188, 1198, 1205, 1205, 1238, 1238, 1238, 1241, 1242, 1244, 1249, 1249, 1249, 1256, 1262, 1262, 1262, 1264, 1264, 1264, 1273, 1273, 1278, 1290, 1290, 1302.	106 O-Glicosilación sites: Positions 16, 25, 128, 183, 185, 190, 191, 194, 203, 226, 229, 238, 244, 245, 249, 251, 268, 272, 275, 276, 279, 280, 283, 287, 290, 292, 305, 325, 329, 330, 332, 358, 363, 364, 365, 367, 387, 493, 497, 504, 538, 551, 557, 561, 562, 563, 564, 566, 567, 582, 583, 586, 588, 593, 594, 595, 597, 604, 617, 620, 658, 705, 710, 724, 728, 730, 815, 822, 826, 828, 829, 831, 832, 835, 843, 848, 853, 857, 858, 860, 861, 865, 879, 887, 892, 895, 901, 905, 909, 911, 915, 937, 938, 949, 1179, 1188, 1238, 1241, 1242, 1243, 1244, 1246, 1249, 1256, 1262).	6 N-Glicosilación sites: Positions 309 NKSE (0,6999) 565 NTKK (0,5121) 694 NLSG (0,5093) 830 NSSA (0,5031) 939 NDSD (0,5029) 1176 NKTS (0,5162)
SPAG9 Tyr914Ter	191 phosphorylation sites: Positions 9, 21, 21, 25, 30, 30, 32, 87, 109, 109, 109, 119, 119, 119, 123, 123, 126, 126, 143, 143, 183, 183, 183, 185, 185, 194, 194, 203, 203, 217, 217, 226, 226, 238, 238, 242, 244, 245, 245, 249, 251, 268, 268, 268, 268, 268, 272, 272, 275, 276, 276, 276, 279, 283, 292, 305, 305, 329, 330, 332, 332, 332, 339, 339, 339, 347, 347, 347, 348, 358, 363, 363, 364, 365, 379, 381, 381, 381, 387, 388, 391, 391, 418, 493, 493, 497, 504, 504, 504, 538, 538, 550, 550, 550, 551, 551, 551, 557, 561, 561, 562, 563, 564, 564, 564, 566, 566, 567, 567, 578, 582, 582, 583, 586, 586, 588, 588, 593, 593, 594, 594, 594, 595, 595, 595, 597, 611, 614, 617, 620, 620, 629, 683, 684, 705, 705, 710, 713, 728, 730, 730, 730, 732, 732, 733, 733, 756, 763, 764, 790, 804, 804, 806, 806, 813, 815, 822, 826, 829, 831, 832, 835, 837, 837, 848, 858, 858, 858, 858, 858, 861, 865, 865, 865, 879, 879, 887, 892, 895, 901, 901, 905, 909, 909.	82 O-Glicosilación sites: Positions 25, 128, 183, 185, 190, 191, 194, 203, 226, 229, 238, 244, 245, 249, 251, 268, 272, 275, 276, 279, 280, 283, 287, 290, 292, 305, 325, 329, 330, 332, 358, 363, 364, 365, 367, 387, 493, 497, 504, 538, 551, 557, 561, 562, 563, 564, 566, 567, 582, 583, 586, 588, 593, 594, 595, 597, 604, 617, 620, 658, 710, 724, 728, 730, 732, 815, 826, 828, 829, 835, 853, 857, 858, 860, 861, 865, 879, 887, 892, 895, 901.	1 N-Glicosilación site: Position 309 NKSE (0,6928)

Comparison between primary sequences of two proteins (wild-type and mutated) according to phosphorylation, O-glycosylation and N-glycosylation sites.



Table 4. Positions phosphorylated by kinases that interact with *SPAG9wt* and the effect of *SPAG9Tyr914Ter*

Positions phosphorylated by kinases in <i>SPAG9</i> (wild-type) are not present in <i>SPAG9Tyr914Ter</i>					
Position	Amino acid	Enzyme	Position	Amino acid	Enzyme
909	S	ATM	1149	T	PKA
909	S	DNA-PK	1149	T	cdc2
909	S	CKI	1169	S	PKA
932	S	unsp	1173	T	PKC
935	Y	SRC	1175	T	PKC
937	S	unsp	1188	S	unsp
944	Y	unsp	1188	S	PKA
944	Y	INSR	1188	S	PKC
966	S	PKA	1198	S	unsp
966	S	cdc2	1205	T	PKC
967	S	cdc2	1205	T	PKG
986	S	PKC	1238	S	p38MAPK
996	S	unsp	1238	S	cdk5
996	S	PKC	1238	S	GSK3
1002	S	unsp	1241	S	unsp
1021	T	DNA-PK	1242	S	unsp
1036	S	cdc2	1244	S	unsp
1049	S	unsp	1249	T	PKC
1049	S	PKA	1249	T	unsp
1054	T	unsp	1249	T	cdc2
1054	T	PKC	1256	S	unsp
1069	Y	unsp	1262	S	unsp
1081	S	unsp	1262	S	DNAPK
1081	S	PKC	1262	S	ATM
1090	S	unsp	1264	T	unsp
1090	S	PKA	1264	T	cdk5
1105	S	PKC	1264	T	p38MAPK
1110	S	RSK	1273	S	unsp
1111	T	PKC	1273	S	CKII
1111	T	unsp	1278	Y	unsp
1131	Y	unsp	1290	S	CKII
1138	T	PKC	1290	S	cdc2
1144	S	cdc2	1302	S	cdc2

Sixty-six lost phosphorylation sites of the mutated protein due to the spatial effect from position 909 (unsp = unspecific enzyme, S = serine, T = threonine, Y = tyrosine).

subtype specification, axon extension and branching, dendrite formation, neurotransmitters, synaptogenesis and synaptic function and axon regeneration (64).

Synaptic dysfunction appears to be relevant in the absence of JIP4. Alterations in the JIP4 scaffold protein can directly impact synapses, mainly at the presynaptic but also at the postsynaptic levels (65, 66). The transport of neurotrophic factors necessary for the formation and maintenance of synapses at the presynaptic level and the postsynaptic level seems to involve the activity of lysosomes responsible for synaptic organization and neuronal pruning.

Recent report demonstrated that axonal lysosomal transport is altered by the loss of JIP4. JIP4/JIP3 could also be regulating the structure and dynamics of the neuronal cytoskeleton (58). Studies in mouse motor neurons concludes that adequate lysosomal activity is key to natural synapse elimination in mouse motor neuron (67). Authors have suggested possible common mechanisms for this regulation in nervous system both at the peripheral and central levels, during neuronal pruning and elimination of axonal connections to cause synaptic refinement (68).

Multiple Mendelian mutations, they have been associated with defects in motor proteins, adapters, or regulators of axonal transport (65). Some neurodevelopmental diseases involved specifically with proteins with functions in retrograde transport previously identified (9) are summarized below. Genetic alterations in the dynein cytoplasmic 1 heavy chain 1 (*DYNC1H1* gene) with associated phenotypes: Charcot-Marie-Tooth disease, axonal, type 20, cortical dysplasia, complex, with other brain malformations 13 and spinal muscular atrophy, lower extremity-predominant 1. Mutations in regulators (*NDE1* and *BICD2*) have been reported (69). *NDE1* is associated to lissencephaly 4 (with microcephaly) and microhydranencephaly. *BICD2*-associated phenotypes are spinal muscular atrophy, lower extremity-predominant, 2A and 2B. *PAFAH1B1* or *LYS 1* is also an important gene required for dynein and microtubule dependent processes, and it is associated with lissencephaly type 1 (70). All of these phenotypes seem to involve more severe and earlier changes in brain development than the phenotype presented here, with clear malformations of cerebral cortical development (MCD) (71). In our cases, no MCD patterns were evident in the neuroimaging.

How Does Defective Retrograde Axonal Transport Contribute to Neurodegenerative Diseases?

Lysosomes recycle or eliminate damaged or misfolded proteins as they travel to the neuronal soma via retrograde axonal transport. Retrograde transport of lysosomes is recognized as an important regulator of autophagy. Autophagy maintains homeostasis and prevents the accumulation of toxic material within the cell. Neurons are particularly sensitive to this toxic accumulation (72). Multiple neurodegenerative diseases

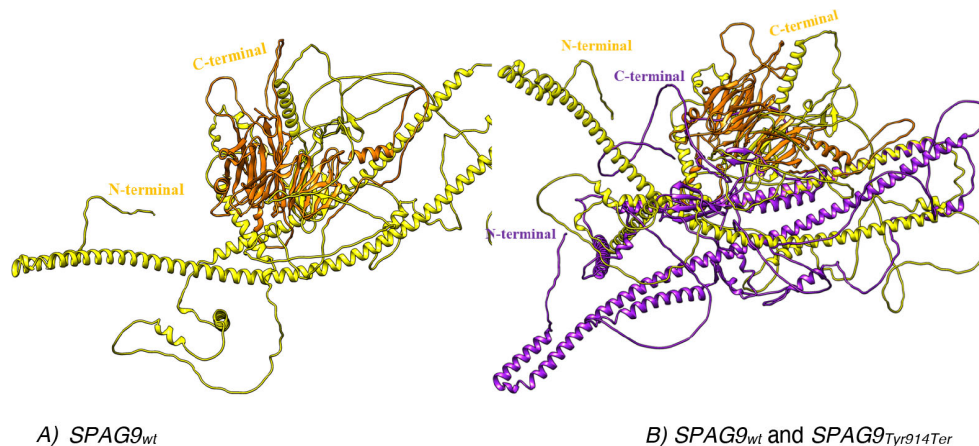


Figure 4. Representation of the three-dimensional model in tapes. (A) Region of the *SPAG9wt* protein after position 914 (in yellow and orange). (B) *SPAG9wt* and *SPAG9Tyr914Ter* (violet) proteins. There was no alignment of the structures. The effect of the charges of the amino acids was lost, affecting their folding and inducing changes in angles that alter the functional interaction.



have been related to defects in axonal transport, including Alzheimer disease (AD), Parkinson's disease, ALS, Huntington disease, frontotemporal dementia, Perry syndrome, Charcot-Marie-Tooth type 2B, among others (73). Autophagy is the process by which aged or toxic proteins and organelles are engulfed by the membrane forming an autophagosome that then fuses with a lysosome to form an autolysosome, with the aim of degrading the contents of the vesicle by lysosomal hydrolases. Lysosomal retrograde transport regulates autophagic flux by facilitating the formation of autophagosomes and fusion between autophagosomes and lysosomes (72). JIP4 phosphorylation acts as a switch that controls lysosomal distribution signaling pathways depending on the type of autophagy-inducing signal (72). Axonal transport of autophagosomes is regulated by JIP4 (74).

There is evidence of JIP3 the homolog of JIP4 and its role in neurodegeneration. The absence of JIP3 showed alteration in zebrafish retrograde transport and lysosome accumulation (75). And in dystrophic axons of the Jip3 KO mouse, immature lysosomes were found in the cell body (76). It has been seen that blocking retrograde transport leads to poor maturation and degradation of lysosomes contributes to their axonal accumulation and altered maturation in axonal inflammations of AD. In JIP3 KO mouse neurons, AD-like accumulations of lysosomes were identified (76) and in JIP3 +/- had worsening amyloid plaque pathology. These results show the importance of JIP3-dependent axonal lysosome transport in regulating amyloid precursor protein processing; however, in the 19 unrelated individuals with de novo variants in JIP3, with intellectual disability phenotype and brain malformations; no subsequent neurodegenerative changes or signs of developmental regression were described (61, 62). This characteristic was also not mentioned in a recent case report (77).

Our three cases are on average 34 years old and follow-up for more than 10 years with worsening cognitive and behavioral function has corroborated progressive cognitive deterioration. We did not find similar findings in the literature caused by dysfunction in the retrograde transport machinery or axonal transport in general, where cases with progressive phenotype, with neurodevelopmental disease and subsequent central neurodegeneration phenotype, are reported (9).

These observations generate multiple questions whose future answers could explain the described family's causal pathological mechanisms and many other diseases involved in cerebral retrograde transport, where development and degeneration tautologically converge.

Declaration of Possible Conflicts of Interests: All contributors have confirmed that no conflict of interest exists.

Author Contributions

N.A.-B. and C.A.V.-L. had full access to all the data in the study.

- Study concept and design: N.A.-B., J.T.-M., L.M., and C.A.V.-L.
- Acquisition, analysis, or interpretation of data: N.A.-B., J.T.-M., A.S.-O., A.M., M.P., and J.N.-T.
- Drafting the manuscript: N.A.-B. and M.A.-B.
- Critical revision of the manuscript for important intellectual content: M.A.C., W.R., G.P.C., and M.A.-B.
- Bioinformatic and structural analysis: N.A.-B., J.T.-M., and A.S.-O.
- Obtaining funding and Study supervision: C.A.V.-L. and M.A.-B.

Data Availability

The datasets used and analyzed during the current study are available from the corresponding author upon reasonable request.

Acknowledgments

Study supported by Universidad de Antioquia and MINCIENCIAS grant number 1115-807-63223, Republic of Colombia. This work is dedicated to the memory of Professor Gabriel Bedoya. We especially thank Professor Sergio Vargas for his contributions in reading the brain MRI, the members of the GENMOL and the GNA groups who helped in some way to make this study possible, and the family studied for their availability and trust.

References

1. Jongsma MLM, Bakker N, Neeffjes J. Choreographing the motor-driven endosomal dance. *J Cell Sci.* 2023;136(5):jcs259689. DOI: [10.1242/jcs.259689](https://doi.org/10.1242/jcs.259689). PMID: 36382597; PMCID: [PMC9845747](https://pubmed.ncbi.nlm.nih.gov/PMC9845747/)
2. Guedes-Dias P, Holzbaur ELF. Axonal transport: driving synaptic function. *Science.* 2019;366:eaaw9997. DOI: [10.1126/science.aaw9997](https://doi.org/10.1126/science.aaw9997). PMID: 31601744; PMCID: [PMC6996143](https://pubmed.ncbi.nlm.nih.gov/PMC6996143/)
3. Hirokawa N, Sato-Yoshitake R, Kobayashi N, Pfister KK, Bloom GS, Brady ST. Kinesin associates with anterogradely transported membranous organelles in vivo. *J Cell Biol.* 1991;114(2):295-302. DOI: [10.1083/jcb.114.2.295](https://doi.org/10.1083/jcb.114.2.295). PMID: 1712789; PMCID: [PMC2289077](https://pubmed.ncbi.nlm.nih.gov/PMC2289077/)
4. Hirokawa N, Sato-Yoshitake R, Yoshida T, Kawashima T. Brain dynein (MAP1C) localizes on both anterogradely and retrogradely transported membranous organelles in vivo. *J Cell Biol.* 1990;111(3):1027-37. DOI: [10.1083/jcb.111.3.1027](https://doi.org/10.1083/jcb.111.3.1027). PMID: 2143999; PMCID: [PMC2116262](https://pubmed.ncbi.nlm.nih.gov/PMC2116262/)
5. Guillaud L, El-Agamy SE, Otsuki M, Terenzio M. Anterograde axonal transport in neuronal homeostasis and disease. *Front Mol Neurosci.* 2020;13:556175. DOI: [10.3389/fnmol.2020.556175](https://doi.org/10.3389/fnmol.2020.556175). PMID: 33071754; PMCID: [PMC7531239](https://pubmed.ncbi.nlm.nih.gov/PMC7531239/)
6. Yamashita N. Retrograde signaling via axonal transport through signaling endosomes. *J Pharmacol Sci.* 2019;141(2):91-6. DOI: [10.1016/j.jphs.2019.10.001](https://doi.org/10.1016/j.jphs.2019.10.001). PMID: 31679963; PMCID: [PMC7531239](https://pubmed.ncbi.nlm.nih.gov/PMC7531239/)
7. Berth SH, Lloyd TE. Disruption of axonal transport in neurodegeneration. *J Clin Invest.* 2023;133:e168554. DOI: [10.1172/JCI168554](https://doi.org/10.1172/JCI168554). PMID: 37259916; PMCID: [PMC10232001](https://pubmed.ncbi.nlm.nih.gov/PMC10232001/)
8. Millicamps S, Julien JP. Axonal transport deficits and neurodegenerative diseases. *Nat Rev Neurosci.* 2013;14(3):161-76. DOI: [10.1038/nrn3380](https://doi.org/10.1038/nrn3380). PMID: 23361386
9. Sleight JN, Rossor AM, Fellows AD, Tosolini AP, Schiavo G. Axonal transport and neurological disease. *Nat Rev Neurol.* 2019;15(12):691-703. DOI: [10.1038/s41582-019-0257-2](https://doi.org/10.1038/s41582-019-0257-2). PMID: 31558780
10. Kelkar N, Standen CL, Davis RJ. Role of the JIP4 scaffold protein in the regulation of mitogen-activated protein kinase signaling pathways. *Mol Cell Biol.* 2005;25(7):2733-43. DOI: [10.1128/MCB.25.7.2733-2743.2005](https://doi.org/10.1128/MCB.25.7.2733-2743.2005). PMID: 15767678; PMCID: [PMC1061651](https://pubmed.ncbi.nlm.nih.gov/PMC1061651/)
11. Dumrongprechachan V, Salisbury RB, Butler L, MacDonald ML, Kozorovitskiy Y. Dynamic proteomic and phosphoproteomic atlas of corticostriatal axons in neurodevelopment. *Elife.* 2022;11:e78847. DOI: [10.7554/eLife.78847](https://doi.org/10.7554/eLife.78847). PMID: 36239373; PMCID: [PMC9629834](https://pubmed.ncbi.nlm.nih.gov/PMC9629834/)
12. Montagnac G, Sibarita JB, Loubéry S, Daviet L, Romao M, Raposo G, et al. ARF6 Interacts with JIP4 to control a motor switch mechanism regulating endosome traffic in cytokinesis. *Curr Biol.* 2009;19(3):184-95. DOI: [10.1016/j.cub.2008.12.043](https://doi.org/10.1016/j.cub.2008.12.043). PMID: 19211056
13. Sato T, Ishikawa M, Mochizuki M, Ohta M, Ohkura M, Nakai J, et al. JSAP1/JIP3 and JLP regulate kinesin-1-dependent axonal transport to prevent neuronal degeneration. *Cell Death Differ.* 2015;22(8):1260-74. DOI: [10.1038/cdd.2014.207](https://doi.org/10.1038/cdd.2014.207). PMID: 25571974; PMCID: [PMC4495352](https://pubmed.ncbi.nlm.nih.gov/PMC4495352/)
14. Cason SE, Holzbaur ELF. Axonal transport of autophagosomes is regulated by dynein activators JIP3/JIP4 and ARF/RAB GTPases. *bioRxiv* 2023. DOI: [10.1101/2023.01.28.526044](https://doi.org/10.1101/2023.01.28.526044). PMCID: [PMC9901177](https://pubmed.ncbi.nlm.nih.gov/PMC9901177/)
15. Yang P, Qiao Y, Meng M, Zhou Q. Cancer/testis antigens as biomarker and target for the diagnosis, prognosis, and therapy of lung cancer. *Front Oncol.* 2022;12:864159. DOI: [10.3389/fonc.2022.864159](https://doi.org/10.3389/fonc.2022.864159). PMID: 35574342; PMCID: [PMC9092596](https://pubmed.ncbi.nlm.nih.gov/PMC9092596/)
16. Acosta-Baena N, Tejada-Moreno JA, García AM, Caro MA, Villegas -Lanau CA, Bedoya-Berrio G. Deletion of the SPAG9 gene cause autosomal-recessive intellectual disability. *General Neuroscience.* 2021;17(S12):e058215. DOI: [10.1002/alz.058215](https://doi.org/10.1002/alz.058215)
17. Wechsler D. The measurement of adult intelligence (3rd ed.). Baltimore: Williams & Wilkins Co; 1946.
18. Acosta-Baena N, Sepulveda-Falla D, Lopera-Gómez CM, Jaramillo-Elorza MC, Moreno S, Aguirre-Acevedo DC, et al. Pre-dementia clinical stages in presenilin 1 E280A familial early-onset Alzheimer's disease: a retrospective cohort study. *Lancet Neurol.* 2011;10(3):213-20. DOI: [10.1016/S1474-4422\(10\)70323-9](https://doi.org/10.1016/S1474-4422(10)70323-9). PMID: 21296022
19. Miller SA, Dykes DD, Polesky HF. A simple salting out procedure for extracting DNA from human nucleated cells. *Nucleic Acids Res.* 1988;16(3):1215. DOI: [10.1093/nar/16.3.1215](https://doi.org/10.1093/nar/16.3.1215). PMID: 3344216; PMCID: [PMC334765](https://pubmed.ncbi.nlm.nih.gov/PMC334765/)
20. Chen R, Im H, Snyder M. Whole-exome enrichment with the agile SureSelect human all exon platform. *Cold Spring Harb Protoc.* 2015;2015(7):626-33. DOI: [10.1101/pdb.prot083659](https://doi.org/10.1101/pdb.prot083659). PMID: 25762417; PMCID: [PMC4490097](https://pubmed.ncbi.nlm.nih.gov/PMC4490097/)
21. Illumina. bcl2fastq conversion software v1.8.4 user guide. 2013. Available from: https://support.illumina.com/sequencing/sequencing_software/bcl2fastq-conversion-software.html.
22. FASTQC SAA quality control tool for high throughput sequence data. 2010.



23. Li H, Durbin R. Fast and accurate short read alignment with Burrows-Wheeler transform. *Bioinformatics*. 2009;25(14):1754–60. DOI: [10.1093/bioinformatics/btp324](https://doi.org/10.1093/bioinformatics/btp324). PMID: 19451168; PMCID: [PMC2705234](https://pubmed.ncbi.nlm.nih.gov/PMC2705234/)
24. DePristo MA, Banks E, Poplin R, Garimella K V, Maguire JR, Hartl C, et al. A framework for variation discovery and genotyping using next-generation DNA sequencing data. *Nat Genet*. 2011;43(5):491–8. DOI: [10.1038/ng.806](https://doi.org/10.1038/ng.806). PMID: 21478889; PMCID: [PMC3083463](https://pubmed.ncbi.nlm.nih.gov/PMC3083463/)
25. Chang X, Wang K. wANNOVAR: annotating genetic variants for personal genomes via the web. *J Med Genet*. 2012;49(7):433–6. DOI: [10.1136/jmedgenet-2012-100918](https://doi.org/10.1136/jmedgenet-2012-100918). PMID: 22717648; PMCID: [PMC3556337](https://pubmed.ncbi.nlm.nih.gov/PMC3556337/)
26. McLaren W, Gil L, Hunt SE, Riat HS, Ritchie GRS, Thormann A, et al. The ensembl variant effect predictor. *Genome Biol*. 2016;17(1):122. DOI: [10.1186/s13059-016-0974-4](https://doi.org/10.1186/s13059-016-0974-4). PMID: 27268795; PMCID: [PMC4893825](https://pubmed.ncbi.nlm.nih.gov/PMC4893825/)
27. Richards S, Aziz N, Bale S, Bick D, Das S, Gastier-Foster J, et al. Standards and guidelines for the interpretation of sequence variants: a joint consensus recommendation of the American College of Medical Genetics and Genomics and the Association for Molecular Pathology. *Genet Med*. 2015;17(5):405–24. DOI: [10.1038/gim.2015.30](https://doi.org/10.1038/gim.2015.30). PMID: 25741868; PMCID: [PMC4544753](https://pubmed.ncbi.nlm.nih.gov/PMC4544753/)
28. Li Q, Wang K. InterVar: clinical interpretation of genetic variants by the 2015 ACMG-AMP guidelines. *Am J Hum Genet*. 2017;100(2):267–80. DOI: [10.1016/j.ajhg.2017.01.004](https://doi.org/10.1016/j.ajhg.2017.01.004). PMID: 28132688; PMCID: [PMC5294755](https://pubmed.ncbi.nlm.nih.gov/PMC5294755/)
29. Kopyanov S, Tsiolkas V, Kouris A, Chapple CE, Aguilera MA, Meyer R, et al. VarSome: the human genomic variant search engine. *Bioinformatics*. 2019;35(11):1978–80. DOI: [10.1093/bioinformatics/bty897](https://doi.org/10.1093/bioinformatics/bty897). PMID: 30376034; PMCID: [PMC6546127](https://pubmed.ncbi.nlm.nih.gov/PMC6546127/)
30. Larsson A. AliView: a fast and lightweight alignment viewer and editor for large datasets. *Bioinformatics*. 2014;30(22):3276–8. DOI: [10.1093/bioinformatics/btu531](https://doi.org/10.1093/bioinformatics/btu531). PMID: 25095880; PMCID: [PMC4221126](https://pubmed.ncbi.nlm.nih.gov/PMC4221126/)
31. Weckx S, Del-Favero J, Rademakers R, Claes L, Cruts M, De Jonghe P, et al. novoSNP, a novel computational tool for sequence variation discovery. *Genome Res*. 2005;15(3):436–42. DOI: [10.1101/gr.2754005](https://doi.org/10.1101/gr.2754005). PMID: 15741513; PMCID: [PMC551570](https://pubmed.ncbi.nlm.nih.gov/PMC551570/)
32. Blom N, Sicheritz-Pontén T, Gupta R, Gammeltoft S, Brunak S. Prediction of post-translational glycosylation and phosphorylation of proteins from the amino acid sequence. *Proteomics*. 2004;4(6):1633–49. DOI: [10.1002/pmic.200300771](https://doi.org/10.1002/pmic.200300771). PMID: 15174133
33. Steentoft C, Vakhrushev SY, Joshi HJ, Kong Y, Vester-Christensen MB, Schjoldager KTBG, et al. Precision mapping of the human O-GalNAc glycoproteome through SimpleCell technology. *EMBO J*. 2013;32(10):1478–88. DOI: [10.1038/emboj.2013.79](https://doi.org/10.1038/emboj.2013.79). PMID: 23584533; PMCID: [PMC3655468](https://pubmed.ncbi.nlm.nih.gov/PMC3655468/)
34. Gupta R, Brunak S. Prediction of glycosylation across the human proteome and the correlation to protein function. *Pac Symp Biocomput*. 2002;322:310–22. PMID: 11928486
35. Isabet T, Montagnac G, Regazzoni K, Raynal B, El Khadali F, England P, et al. The structural basis of Arf effector specificity: the crystal structure of ARF6 in a complex with JIP4. *EMBO J*. 2009;28(18):2835–45. DOI: [10.1038/emboj.2009.209](https://doi.org/10.1038/emboj.2009.209). PMID: 19644450; PMCID: [PMC2750013](https://pubmed.ncbi.nlm.nih.gov/PMC2750013/)
36. Jumper J, Evans R, Pritzel A, Green T, Figurnov M, Ronneberger O, et al. Highly accurate protein structure prediction with AlphaFold. *Nature*. 2021;596(7873):583–9. DOI: [10.1038/s41586-021-03819-2](https://doi.org/10.1038/s41586-021-03819-2). PMID: 34265844; PMCID: [PMC8371605](https://pubmed.ncbi.nlm.nih.gov/PMC8371605/)
37. López-Rivera JJ, Rodríguez-Salazar L, Soto-Ospina A, Estrada-Serrato C, Serrano D, Chaparro-Solano HM, et al. Structural protein effects underpinning cognitive developmental delay of the PURA p.Phe233del mutation modelled by artificial intelligence and the hybrid quantum mechanics–molecular mechanics framework. *Brain Sci*. 2022;12(7):871. DOI: [10.3390/brainsci12070871](https://doi.org/10.3390/brainsci12070871). PMID: 35884678; PMCID: [PMC9313109](https://pubmed.ncbi.nlm.nih.gov/PMC9313109/)
38. Varadi M, Anyango S, Deshpande M, Nair S, Natassia C, Yordanova G, et al. AlphaFold protein structure database: massively expanding the structural coverage of protein–sequence space with high-accuracy models. *Nucleic Acids Res*. 2022;50(D1):D439–44. DOI: [10.1093/nar/gkab1061](https://doi.org/10.1093/nar/gkab1061). PMID: 34791371; PMCID: [PMC8728224](https://pubmed.ncbi.nlm.nih.gov/PMC8728224/)
39. Pettersen EF, Goddard TD, Huang CC, Couch GS, Greenblatt DM, Meng EC, et al. UCSF Chimera - a visualization system for exploratory research and analysis. *J Comput Chem*. 2004;25(13):1605–12. DOI: [10.1002/jcc.20084](https://doi.org/10.1002/jcc.20084). PMID: 15264254
40. Garel C, Cont I, Alberti C, Josserand E, Moutard ML, Le Pointe HD. Biometry of the corpus callosum in children: MR imaging reference data. *Am J Neuroradiol*. 2011;32(8):1436–43. DOI: [10.3174/ajnr.A2542](https://doi.org/10.3174/ajnr.A2542). PMID: 21799035; PMCID: [PMC7964359](https://pubmed.ncbi.nlm.nih.gov/PMC7964359/)
41. UniProt Consortium. UniProt: the universal protein knowledgebase in 2023. *Nucleic Acids Res*. 2023;51:523–31. DOI: [10.1093/nar/gkac1052](https://doi.org/10.1093/nar/gkac1052). PMID: 36408920; PMCID: [PMC9825514](https://pubmed.ncbi.nlm.nih.gov/PMC9825514/)
42. Apweiler R, Bateman A, Martin MJ, O'Donovan C, Magrane M, Alam-Faruque Y, et al. Activities at the universal protein resource (UniProt). *Nucleic Acids Res*. 2014;42(D1):191–8. DOI: [10.1093/nar/gkt1140](https://doi.org/10.1093/nar/gkt1140). PMID: 24253303; PMCID: [PMC3965022](https://pubmed.ncbi.nlm.nih.gov/PMC3965022/)
43. UniProt Consortium. Reorganizing the protein space at the Universal Protein Resource (UniProt). *Nucleic Acids Res*. 2012;40(2):D71–5. DOI: [10.1093/nar/gkr981](https://doi.org/10.1093/nar/gkr981). PMID: 22102590; PMCID: [PMC3245120](https://pubmed.ncbi.nlm.nih.gov/PMC3245120/)
44. Celestino R, Gama JB, Castro-Rodrigues AF, Barbosa DJ, Rocha H, d'Amico EA, et al. JIP3 interacts with dynein and kinesin-1 to regulate bidirectional organelle transport. *J Cell Biol*. 2022;221(8):e202110057. DOI: [10.1083/jcb.202110057](https://doi.org/10.1083/jcb.202110057). PMID: 35829703; PMCID: [PMC9284427](https://pubmed.ncbi.nlm.nih.gov/PMC9284427/)
45. Mooney JA, Huber CD, Service S, Sul JH, Marsden CD, Zhang Z, et al. Understanding the hidden complexity of Latin American population isolates. *Am J Hum Genet*. 2018;103(5):707–26. DOI: [10.1016/j.ajhg.2018.09.013](https://doi.org/10.1016/j.ajhg.2018.09.013). PMID: 30401458; PMCID: [PMC6218714](https://pubmed.ncbi.nlm.nih.gov/PMC6218714/)
46. Carvajal-Carmona LG, Ophoff R, Service S, Hartiala J, Molina J, Leon P, et al. Genetic demography of antioquia (Colombia) and the central valley of costa rica. *Hum Genet*. 2003;112(5–6):534–41. DOI: [10.1007/s00439-002-0899-8](https://doi.org/10.1007/s00439-002-0899-8). PMID: 12601469
47. Cardoso-dos-Santos AC, Reales G, Schuler-Faccini L. Clusters of rare disorders and congenital anomalies in South America. *Rev Panam Salud Pública*. 2023;47:e98. DOI: [10.26633/RPSP.2023.98](https://doi.org/10.26633/RPSP.2023.98). PMID: 37363626; PMCID: [PMC10289474](https://pubmed.ncbi.nlm.nih.gov/PMC10289474/)
48. Bajić D, Moreira NC, Wikström J, Raininko R. Asymmetric development of the hippocampal region is common: a fetal MR imaging study. *Am J Neuroradiol*. 2012;33(3):513–8. DOI: [10.3174/ajnr.A2814](https://doi.org/10.3174/ajnr.A2814). PMID: 22116115; PMCID: [PMC7966435](https://pubmed.ncbi.nlm.nih.gov/PMC7966435/)
49. Fu TY, Ho CR, Lin CH, Lu YT, Lin WC, Tsai MH. Hippocampal malrotation: a genetic developmental anomaly related to epilepsy? *Brain Sci*. 2021;11(4):463. DOI: [10.3390/brainsci11040463](https://doi.org/10.3390/brainsci11040463). PMID: 33916495; PMCID: [PMC8067421](https://pubmed.ncbi.nlm.nih.gov/PMC8067421/)
50. Blaauw J, Meiners LC. The splenium of the corpus callosum: embryology, anatomy, function and imaging with pathophysiological hypothesis. *Neuroradiology*. 2020;62:563–85. DOI: [10.1007/s00234-019-02357-z](https://doi.org/10.1007/s00234-019-02357-z). PMID: 32062761; PMCID: [PMC7186255](https://pubmed.ncbi.nlm.nih.gov/PMC7186255/)
51. Keshavan MS, Diwadkar VA, DeBellis M, Dick E, Kotwal R, Rosenberg DR, et al. Development of the corpus callosum in childhood, adolescence and early adulthood. *Life Sci*. 2002;70(16):1909–22. DOI: [10.1016/s0024-3205\(02\)01492-3](https://doi.org/10.1016/s0024-3205(02)01492-3). PMID: 12005176
52. Cerasuolo M, Di Meo I, Auriemma MC, Trojsi F, Maiorino MI, Cirillo M, et al. Iron and ferroptosis more than a suspect: beyond the most common mechanisms of neurodegeneration for new therapeutic approaches to cognitive decline and dementia. *Int J Mol Sci*. 2023;24(11):9637. DOI: [10.3390/ijms24119637](https://doi.org/10.3390/ijms24119637). PMID: 37298586; PMCID: [PMC10253771](https://pubmed.ncbi.nlm.nih.gov/PMC10253771/)
53. Asih PR, Prikas E, Stefanoska K, Tan ARP, Ahel HI, Ittner A. Functions of p38 MAP kinases in the central nervous system. *Front Mol Neurosci*. 2020;13:570586. DOI: [10.3389/fnmol.2020.570586](https://doi.org/10.3389/fnmol.2020.570586). PMID: 33013322; PMCID: [PMC7509416](https://pubmed.ncbi.nlm.nih.gov/PMC7509416/)
54. Gibbs KL, Greensmith L, Schiavo G. Regulation of axonal transport by protein kinases. *Trends Biochem Sci*. 2015;40:597–610. DOI: [10.1016/j.tibs.2015.08.003](https://doi.org/10.1016/j.tibs.2015.08.003). PMID: 26410600
55. Tortarolo M, Veglianesi P, Calvaresi N, Botturi A, Rossi C, Giorgini A, et al. Persistent activation of p38 mitogen-activated protein kinase in a mouse model of familial amyotrophic lateral sclerosis correlates with disease progression. *Mol Cell Neurosci*. 2003;23(2):180–92. DOI: [10.1016/s1044-7431\(03\)00022-8](https://doi.org/10.1016/s1044-7431(03)00022-8). PMID: 12812752
56. Ballabio A, Bonifacino JS. Lysosomes as dynamic regulators of cell and organismal homeostasis. *Nat Rev Mol Cell Biol*. 2020;21(2):101–18. DOI: [10.1038/s41580-019-0185-4](https://doi.org/10.1038/s41580-019-0185-4). PMID: 31768005
57. Willett R, Martina JA, Zewe JP, Wills R, Hammond GR V, Puertollano R. TFEB regulates lysosomal positioning by modulating TMEM55B expression and JIP4 recruitment to lysosomes. *Nat Commun*. 2017;8(1):1580. DOI: [10.1038/s41467-017-01871-z](https://doi.org/10.1038/s41467-017-01871-z). PMID: 29146937; PMCID: [PMC5691037](https://pubmed.ncbi.nlm.nih.gov/PMC5691037/)
58. Rafiq NM, Lyons LL, Gowrishankar S, De Camilli P, Ferguson SM. JIP3 links lysosome transport to regulation of multiple components of the axonal cytoskeleton. *Commun Biol*. 2022;5(1). DOI: [10.1038/s42003-021-02945-x](https://doi.org/10.1038/s42003-021-02945-x). PMID: 35013510; PMCID: [PMC8748971](https://pubmed.ncbi.nlm.nih.gov/PMC8748971/)
59. Stirnimann CU, Petsalaki E, Russell RB, Müller CW. WD40 proteins propel cellular networks. *Trends Biochem Sci*. 2010;35(10):565–74. DOI: [10.1016/j.tibs.2010.04.003](https://doi.org/10.1016/j.tibs.2010.04.003). PMID: 20451393
60. Gowrishankar S, Lyons L, Rafiq NM, Rocznik-Ferguson A, De Camilli P, Ferguson SM. Overlapping roles of JIP3 and JIP4 in promoting axonal transport of lysosomes in human iPSC-derived neurons. *Mol Biol Cell*. 2021;32(11):1094–103. DOI: [10.1091/mbc.E20-06-0382](https://doi.org/10.1091/mbc.E20-06-0382). PMID: 33788575; PMCID: [PMC8351540](https://pubmed.ncbi.nlm.nih.gov/PMC8351540/)
61. Iwasawa S, Yanagi K, Kikuchi A, Kobayashi Y, Haginoya K, Matsumoto H, et al. Recurrent de novo MAPK8IP3 variants cause neurological phenotypes. *Ann Neurol*. 2019;85(6):927–33. DOI: [10.1002/ana.25481](https://doi.org/10.1002/ana.25481). PMID: 30945334
62. Platzer K, Sticht H, Edwards SL, Allen W, Angione KM, Bonati MT, et al. De novo variants in MAPK8IP3 cause intellectual disability with variable brain anomalies.



- Am J Hum Genet. 2019;104(2):203–12. DOI: [10.1016/j.ajhg.2018.12.008](https://doi.org/10.1016/j.ajhg.2018.12.008). PMID: 30612693; PMCID:PMC6369540.
63. Zweifel LS, Kuruville R, Ginty DD. Functions and mechanisms of retrograde neurotrophin signalling. *Nat Rev Neurosci*. 2005;6:615–25. DOI: [10.1038/nrn1727](https://doi.org/10.1038/nrn1727). PMID: 16062170
64. Harrington AW, Ginty DD. Long-distance retrograde neurotrophic factor signalling in neurons. *Nat Rev Neurosci*. 2013;14(3):177–87. DOI: [10.1038/nrn3253](https://doi.org/10.1038/nrn3253). PMID: 23422909
65. Xiong GJ, Sheng ZH. Presynaptic perspective: axonal transport defects in neurodevelopmental disorders. *J Cell Biol*. 2024;223:e202401145. DOI: [10.1083/jcb.202401145](https://doi.org/10.1083/jcb.202401145). PMID: 38568173; PMCID: [PMC10988239](https://pubmed.ncbi.nlm.nih.gov/PMC10988239/)
66. Exposito-Alonso D, Rico B. Annual review of genetics mechanisms underlying circuit dysfunction in neurodevelopmental disorders. *Annu Rev Genet*. 2022;56:391–422. DOI: [10.1146/annurev-genet-072820-023642](https://doi.org/10.1146/annurev-genet-072820-023642). PMID: 36055969
67. Song JW, Misgeld T, Kang H, Knecht S, Lu J, Cao Y, et al. Lysosomal activity associated with developmental axon pruning. *J Neurosci*. 2008;28(36):8993–9001. DOI: [10.1523/JNEUROSCI.0720-08.2008](https://doi.org/10.1523/JNEUROSCI.0720-08.2008). PMID: 18768693; PMCID: [PMC2693713](https://pubmed.ncbi.nlm.nih.gov/PMC2693713/)
68. Lichtman JW, Colman H. Synapse elimination review and indelible memory. *Neuron*. 2000;25(2):269–78. DOI: [10.1016/s0896-6273\(00\)80893-4](https://doi.org/10.1016/s0896-6273(00)80893-4). PMID: 10719884
69. Lipka J, Kuijpers M, Jaworski J, Hoogenraad CC. Mutations in cytoplasmic dynein and its regulators cause malformations of cortical development and neurodegenerative diseases. *Biochem Soc Trans*. 2013;41(6):1605–12. DOI: [10.1042/BST20130188](https://doi.org/10.1042/BST20130188). PMID: 24256262
70. Reiner O, Carrozzo R, Shen Y, Wehnert M, Faustarella F, Dobyns WB, et al. Isolation of a Miller–Dicker lissencephaly gene containing G protein β -subunit-like repeats. *Nature*. 1993;364(6439):717–21. DOI: [10.1038/364717a0](https://doi.org/10.1038/364717a0). PMID: 8355785
71. Barkovich AJ, Guerrini R, Kuzniecky RI, Jackson GD, Dobyns WB. A developmental and genetic classification for malformations of cortical development: Update 2012. *Brain*. 2012;135:1348–69. DOI: [10.1093/brain/aws019](https://doi.org/10.1093/brain/aws019). PMID: 22427329; PMCID: [PMC3338922](https://pubmed.ncbi.nlm.nih.gov/PMC3338922/)
72. Sasazawa Y, Souma S, Furuya N, Miura Y, Kazuno S, Kakuta S, et al. Oxidative stress-induced phosphorylation of JIP4 regulates lysosomal positioning in coordination with TRPML1 and ALG2. *EMBO J*. 2022;41(22):e111476. DOI: [10.15252/embj.2022111476](https://doi.org/10.15252/embj.2022111476). PMID: 36394115; PMCID: [PMC9670204](https://pubmed.ncbi.nlm.nih.gov/PMC9670204/)
73. Perlson E, Maday S, Fu MM, Moughamian AJ, Holzbaur ELF. Retrograde axonal transport: pathways to cell death? *Trends Neurosci*. 2010;33:335–44. DOI: [10.1016/j.tins.2010.03.006](https://doi.org/10.1016/j.tins.2010.03.006). PMID: 20434225; PMCID: [PMC2902719](https://pubmed.ncbi.nlm.nih.gov/PMC2902719/)
74. Cason SE, Holzbaur ELF. Axonal transport of autophagosomes is regulated by dynein activators JIP3/JIP4 and ARF/RAB GTPases. *J Cell Biol*. 2023;222(12):e202301084. DOI: [10.1016/j.tins.2010.03.006](https://doi.org/10.1016/j.tins.2010.03.006). PMID: 20434225; PMCID: [PMC2902719](https://pubmed.ncbi.nlm.nih.gov/PMC2902719/)
75. Drerup CM, Nechiporuk AV. JNK-interacting protein 3 mediates the retrograde transport of activated c-Jun N-terminal kinase and lysosomes. *PLoS Genet*. 2013;9(2):e1003303. DOI: [10.1371/journal.pgen.1003303](https://doi.org/10.1371/journal.pgen.1003303). PMID: 23468645; PMCID: [PMC3585007](https://pubmed.ncbi.nlm.nih.gov/PMC3585007/)
76. Gowrishankar S, Wu Y, Ferguson SM. Impaired JIP3-dependent axonal lysosome transport promotes amyloid plaque pathology. *J Cell Biol*. 2017;216(10):3291–305. DOI: [10.1083/jcb.201612148](https://doi.org/10.1083/jcb.201612148). PMID: 28784610; PMCID: [PMC5626538](https://pubmed.ncbi.nlm.nih.gov/PMC5626538/)
77. Kárteszi J, Ziegler A, Tihanyi M, Elmont B, Zhang Y, Patócs B, et al. Compound heterozygous variants in MAPK8IP3 were detected in severe congenital hypotonia mimicking lethal spinal muscular atrophy. *Am J Med Genet A*. 2023;191(9):2428–32. DOI: [10.1002/ajmg.a.63340](https://doi.org/10.1002/ajmg.a.63340). PMID: 37462082

Publisher's note: Genomic Press maintains a position of impartiality and neutrality regarding territorial assertions represented in published materials and affiliations of institutional nature. As such, we will use the affiliations provided by the authors, without editing them. Such use simply reflects what the authors submitted to us and it does not indicate that Genomic Press supports any type of territorial assertions.



Open Access. This article is licensed to Genomic Press under the Creative Commons Attribution-NonCommercial-NoDerivatives 4.0 International License (CC BY-NC-ND 4.0). The license mandates: (1) Attribution: Credit must be given to the original work, with a link to the license and notification of any changes. The acknowledgment should not imply licensor endorsement. (2) NonCommercial: The material cannot be used for commercial purposes. (3) NoDerivatives: Modified versions of the work cannot be distributed. (4) No additional legal or technological restrictions may be applied beyond those stipulated in the license. Public domain materials or those covered by statutory exceptions are exempt from these terms. This license does not cover all potential rights, such as publicity or privacy rights, which may restrict material use. Third-party content in this article falls under the article's Creative Commons license unless otherwise stated. If use exceeds the license scope or statutory regulation, permission must be obtained from the copyright holder. For complete license details, visit <https://creativecommons.org/licenses/by-nc-nd/4.0/>. The license is provided without warranties.